Towards a Coordinated Spectral Support Estimation of Sinusoidal Disturbances in Smart Grids through Synchronized Measurements

Carlo Sitzia
Dept. of Electrical and Electronic Eng.
University of Cagliari
Cagliari, Italy
carlo.sitzia@unica.it

David Macii
Dept. of Industrial Engineering
University of Trento
Trento, Italy
david.macii@unitn.it

Paolo Attilio Pegoraro
Dept. of Electrical and Electronic Eng.
University of Cagliari
Cagliari, Italy
paolo.pegoraro@unica.it

Abstract

The increasing diffusion of both large nonlinear loads and renewable-based Distributed Energy Resources may cause serious Power Quality problems, e.g., due to the widespread use of high-efficiency smart power electronics converters (PECs). Despite the considerable effort in mitigating the harmonic distortion injected by these devices, a reliable and accurate detection of the most critical harmonic and interharmonic components affecting a distribution system is essential not only for monitoring, but also for compensation purposes. In this paper, a first step in this direction is proposed. The basic idea is to improve the estimation accuracy of the spectral support of possible sinusoidal disturbances by merging synchronized measurements collected in different points of a grid to better compensate critical harmonics and interharmonics through smart PECs. In particular, a coordinated method based on the local identification of the sinusoidal components in voltage or signal waveforms followed by a weighted average of the frequency estimates of the most significant components in the grid is presented and evaluated through simulations. The reported results confirm the feasibility and the benefits of the coordinated approach.

Index Terms

Phasor Electronic Converters (PECs), Harmonics and interharmonics detection, ESPRIT, frequency estimation, data fusion.

I. Introduction

As known, the growing harmonic distortion affecting voltage and current waveforms due to the penetration of both renewable-based Distributed Energy Resources (DERs) and strongly nonlinear loads poses critical Power Quality (PQ) issues at the distribution level [1], [2]. For instance, the grid-supporting and grid-forming Power Electronics Converters (PECs) play a pivotal role for a flexible and safe grid-integration of DERs [3]. However, they often also tend to inject a large amount of harmonics and inter-harmonics due to the switching electronic devices used for high-efficiency conversion [4], [5]. In fact, even though the most advanced PECs are designed both to mitigate harmonic and inter-harmonic pollution and to cope with significant PQ disturbances [6], [7], poor PQ may still cause, among other drawbacks, the sudden disconnections of DERs, even if advanced anti-islanding systems are used [8].

On the other hand, the PEC controllers may include and provide a variety of functions for voltage regulation, efficient energy exploitation, load balancing, power factor correction, and overload or thermal protection [9]. Moreover, some recent studies have highlighted the potentialities of collaborative PECs to improve grid-forming performance, especially when a multitude of DERs have to be connected to a distribution network [10]. Indeed, harmonic compensation and PQ improvement could be achieved by using the data potentially collected and shared by multiple devices [11]. Of course, this kind of distributed solutions requires that local data acquisition and measurement functions are implemented in heterogeneous smart devices. Indeed, they could and should be used to improve both system observability and monitoring capability as well as to support coordinated control actions. Some relevant examples of this general idea are: the installation of smart meters for PQ monitoring [12], the inclusion of algorithms similar to those commonly used in Phasor Measurement Units (PMUs) into the controller of smart inverters [13], the design of distribution-oriented harmonic PMUs [14], and the increasing diffusion of smart substations [15]. Such upgraded measurement infrastructure could unlock higher-level monitoring applications like harmonic state estimation [16] or harmonic sources identification [17].

In this scenario, this paper explores the feasibility of using coordinated frequency measurements of the sinusoidal components identified in different points of a grid to provide a more accurate estimate of their spectral support for harmonics and interharmonics compensation. In particular, first the ESPRIT-based algorithm described in [18] is applied locally to detect

This work was funded by the European Union – Next Generation EU through the Italian Ministerial grant PRIN 2022 "Smart grid-connected power converters based on advanced synchrophasor-inspired harmonics measurements for holistic integration of renewable energy sources (POWERHERO)," n. 20224X2AYH, CUP F53D23000490006.

the number of sinusoidal components in a voltage or current waveform and their frequencies. Then, the results returned by this algorithm running on different distributed measurement devices at the same time are combined to estimate the spectral support of harmonic and interharmonic disturbances. The final goal is to support grid-wide control actions.

The rest of this paper is structured as follows. In Section II, the algorithm used for detecting and estimating the sinusoidal tones in voltage or signal waveforms is described and the proposed data fusion approach is explained. In Section III some meaningful results are reported. Finally, Section IV concludes the paper and outlines the future work.

II. Sinusoidal Tones Detection and Estimation

The approach adopted in this paper to detect and to estimate the parameters of critical harmonics and interharmonics in different points of a grid is based on the iterative algorithm described in [18]. This algorithm relies on Random Matrix Theory (RMT) and on the Estimation of Signal Parameters via the Rotational Invariance Technique (ESPRIT) [19]. Assuming that K synchronized AC voltage and/or current waveforms are collected all over a grid (either at different locations or in the same point but from a different phase), the sequence of samples of the $k-$th waveform can be modelled as follows, i.e.,

$$x_k(n) = \sum_{d=1}^{D_k} \sqrt{2} A_{k,d}(n) \cos\left(2\pi \frac{f_{k,d}}{f_{s_k}} n + \varphi_{k,d}\right) + \epsilon_k(n) \tag{1}$$

where f_{s_k} is the sampling rate of the $k-$th measurement device, D_k is the unknown number of sinusoidal tones composing the $k-$th waveform; $A_{k,d}$, $f_{k,d}$ and $\varphi_{k,d}$ are the Root Mean Square (RMS) amplitude, the frequency and the initial phase, respectively, of the $d-$th component of the signal for $d = 1, \ldots, D_k$ and $\epsilon_k(\cdot)$ denotes the sequence of normally-distributed zero-mean random noise values with variance σ_k^2. Assuming that all the parameters in (1) are quasi-stationary, if we denote with

$$\mathbf{x}_k(n) = [x_k(n), x_k(n-1), \ldots, x_k(n-M_k+1)]^T \tag{2}$$

(with ^{T} being the transpose operator) the vector of the latest M_k waveform samples, it can be shown that the autocorrelation matrix of $\mathbf{x}_k$ can be expressed and decomposed into singular values as follows, i.e. [19],

$$\begin{aligned} \mathbf{R}_k =& E\{\mathbf{x}_k(n)\mathbf{x}_k^T(n)\} = \mathbf{S}_k \mathbf{\Lambda}_k \mathbf{S}_k^T = \\ & \left[\mathbf{S}_{2D_k}\ \mathbf{S}_{M_k-2D_k}\right] \begin{bmatrix} \frac{M_k}{2}\mathbf{P}_k + \sigma_k^2 \mathbf{I}_{2D_k} & 0 \\ 0 & \sigma_k^2 \mathbf{I}_{M_k-2D_k} \end{bmatrix} \begin{bmatrix} \mathbf{S}_{2D_k}^T \\ \mathbf{S}_{M_k-2D_k}^T \end{bmatrix} \end{aligned} \tag{3}$$

where:

- $E\{\cdot\}$ is the expectation operator.
- $\mathbf{\Lambda}_k$ is the diagonal matrix comprising the singular values of $\mathbf{R}_k$. Such values can be split into two subsets: $2D_k$ of them are approximately proportional to the elements of matrix $\mathbf{P}_k = \text{diag}\left(A_{k,1}^2, A_{k,1}^2, \ldots, A_{k,D_k}^2, A_{k,D_k}^2\right)$ which includes the power values of all the sinusoidal tones, whereas the remaining $M_k - 2D_k$ refer to the noise vector subspace.
- $\mathbf{S}_k$ is the matrix of orthonormal singular vectors associated with the elements of $\mathbf{\Lambda}_k$. Again, the first $2D_k$ columns of $\mathbf{S}_k$ (that are included into matrix $\mathbf{S}_{2D_k}$) refer to the sinusoidal tones, while the singular vectors in $\mathbf{S}_{M_k-2D_k}$ refer to the noise singular values.
- Finally, $\mathbf{I}$ represents the identity matrix of size specified in the subscript.

The singular values and singular vectors resulting from (3) can be used to detect the sinusoidal tones in (1), as well as their frequency and RMS amplitude, as explained in Sections II-A and II-B, respectively. Finally, Section II-C explains how these results can be potentially merged to achieve a better and more reliable grid-area estimation of the actual harmonic and interharmonic content.

A. RMT-based Sinusoidal Tones Detection

Given L_k consecutive data vectors as defined in (2), the maximum likelihood estimator of the autocorrelation matrix (3) is simply

$$\hat{\mathbf{R}}_k = \frac{1}{L_k} \sum_{l=0}^{L_k-1} \mathbf{x}_k(n - l \cdot M_k)\mathbf{x}_k^T(n - l \cdot M_k). \tag{4}$$

This estimate should be refreshed at a quite high rate, e.g., any time a new record of M_k samples is acquired. The values of M_k and L_k have to be as small as possible to keep the initial latency and the overall computational burden low. Also, to ensure that the phase angles of all sinusoidal components in (1) are quite uniformly swept between 0 and 2π at the beginning of different records, M_k must not correspond to an integer number of cycles of any sinusoidal tone. This is a necessary condition to avoid that the estimation of $\mathbf{R}_k$ is biased [18]. Once matrix $\hat{\mathbf{R}}_k$ is estimated through (4), the number of sinusoidal tones can be found by comparing the singular values of the matrix with a threshold that in principle depends on the statistical distribution

of the noise singular values only. The number of singular values that exceed this threshold provides an estimate of D_k. The main steps of this iterative algorithm are briefly recalled below. The details and the underlying theory are instead explained in [18] and [20], [21], respectively.

1) First of all, the singular values of $\hat{\mathbf{R}}_k$ in matrix $\hat{\mathbf{\Lambda}}_k = \mathrm{diag}\left(\hat{\lambda}_{k,1}, \ldots, \hat{\lambda}_{k,M_k}\right)$ are arranged in descending order.
2) Starting from the initial assumption that just the fundamental tone is present in (1) (that is equivalent to assume that $\hat{D}_k = j = 1$), the variance of the noise floor for a given number of sinusoidal tones j is estimated iteratively as follows, i.e.

$$\hat{\sigma}_k^2(j,t) = \frac{1}{M_k - 2j}\left[\sum_{m=2j+1}^{M_k} \hat{\lambda}_{k,m} - \sum_{i=1}^{2j} \rho_{k,i}(t)\right] \quad t \geq 0 \tag{5}$$

where $\hat{\sigma}_k^2(j,0) = \frac{1}{M_k-2j}\sum_{m=2j+1}^{M_k} \hat{\lambda}_{k,m}$ is just the average of the singular values attributed to the noise subspace, and the corrective terms $\rho_{k,i}(t)$ (with $i = 1, \ldots, 2j$) are the larger real-valued solutions of equations

$$\begin{aligned}\rho_{k,i}^2(t) - \rho_{k,i}(t)\left[\hat{\lambda}_{k,i} + \hat{\sigma}_k^2(j,t-1)\left(1 - \tfrac{M_k-2j}{L_k}\right)\right] + \\ + \hat{\lambda}_{k,i}\hat{\sigma}_k^2(j,t-1) = 0\end{aligned} \tag{6}$$

These corrective terms tend to remove the bias affecting the noise variance estimates due to the estimation errors associated with the singular values of the identified sinusoidal tones. Note that equations (5)-(6) must be solved in loop iteratively till when either the values of $\hat{\sigma}_k^2(j,t)$ no longer change significantly (e.g., with variations below $1\,\%$) or the solutions of (6) are no longer real-valued. In such conditions, the estimated noise variance for a given j is referred to as $\hat{\sigma}_{k|j}^2 = \hat{\sigma}_k^2(j,t)$.
3) Leveraging this result, the following hypothesis test is performed, i.e.

$$\begin{aligned}H_0 &: \hat{\lambda}_{k,(2j+1)} \leq T_j \\ H_1 &: \hat{\lambda}_{k,(2j+1)} > T_j\end{aligned} \tag{7}$$

where

$$T_j = \hat{\sigma}_{k|j}^2\left(\mu_{L_k,M_k-2j} + s(\beta)\xi_{L_k,M_k-2j}\right) \tag{8}$$

is a threshold based on the Tracy-Widom distribution of the largest estimated singular value of a pure random noise matrix [21]. In particular, if $\beta << 1$ represents the target false alarm probability (namely the acceptable probability of wrongly detecting a sinusoidal tone), the parameters of (8) result from [21]

$$\begin{aligned}\mu_{L_k,M_k-2j} &= \tfrac{1}{L_k}\left(\sqrt{L_k - \tfrac{1}{2}} + \sqrt{M_k - 2j - \tfrac{1}{2}}\right)^2 \\ \xi_{L_k,M_k-2j} &= \sqrt{\tfrac{\mu_{L_k,M_k-2j}}{L_k}}\left(\tfrac{1}{\sqrt{L_k-\frac{1}{2}}} + \tfrac{1}{\sqrt{M_k-2j-\frac{1}{2}}}\right)^{\frac{1}{3}} \\ s(\beta) &\approx \left(-\tfrac{3}{2}\cdot\log(4\sqrt{\pi}\cdot\beta)\right)^{\frac{2}{3}}\end{aligned} \tag{9}$$

4) If the null hypothesis H_0 is rejected (i.e., H_1 is true), the algorithm starts over by incrementing j by 1. Otherwise, the algorithm ends returning $\hat{D}_k = j$.

B. ESPRIT-based Frequency and RMS Amplitude Estimation

Once the number on sinusoidal components is known, the corresponding singular vectors in $\hat{\mathbf{S}}_{2D_k}$ can be extracted from $\hat{\mathbf{S}}_k$ to build the following two $(M_k - 1) \times 2\hat{D}_k$ matrices, i.e., $\hat{\mathbf{S}}_{D1_k} = [\mathbf{I}_{M_k-1}\ \mathbf{0}]\hat{\mathbf{S}}_{2D_k}$ and $\hat{\mathbf{S}}_{D2_k} = [\mathbf{0}\ \mathbf{I}_{M_k-1}]\hat{\mathbf{S}}_{2D_k}$. Given that in the case of sinusoidal tones $\hat{\mathbf{S}}_{D2_k} = \hat{\mathbf{S}}_{D1_k}\Psi$ where Ψ is a rotation matrix [19], it follows easily that

$$\Psi = (\hat{\mathbf{S}}_{D1_k}^T\hat{\mathbf{S}}_{D1_k})^{-1}\hat{\mathbf{S}}_{D1_k}^T\hat{\mathbf{S}}_{D2_k} \tag{10}$$

Quite importantly, all the eigenvalues $\hat{\tau}_1, \ldots, \hat{\tau}_{2\hat{D}_k}$ of matrix Ψ have unit magnitude, while their phase angles are the normalized positive and negative angular frequencies of the detected sinusoidal components. Therefore, the estimated frequency of such components expressed in Hz are given by

$$\hat{f}_{k,\hat{d}_k} = \frac{f_{s_k}}{2\pi}\left|\arctan2\Big(\mathrm{Im}(\hat{\tau}_{2\hat{d}_k-1}), \mathrm{Re}(\hat{\tau}_{2\hat{d}_k-1})\Big)\right| \qquad \hat{d}_k = 1, \ldots, \hat{D}_k \tag{11}$$

where $\arctan2(y,x)$ is the 2-argument four-quadrant inverse tangent function. Notice that only the odd-indexed eigenvalues of matrix Ψ are considered in (11) because, for each frequency component a pair of complex-conjugate eigenvalues exists.

Therefore, just the absolute value of the phase of one of them is sufficient to extract the estimated frequency. Observe also that the meaning of index $\hat{d}_k$ in (11) may differ from the meaning of index d in (1), since some of the actual components in the $k-$th signal could be misdetected.

The RMS amplitude values of the same sinusoidal components result instead from the singular value decomposition of $\hat{\mathbf{R}}_k$. Indeed, recalling that each pair of singular values associated to the same sinusoidal tone are approximately equal, it follows from (3) that

$$\hat{A}_{k,\hat{d}_k} = \sqrt{\frac{2}{M_k}\left(\frac{\hat{\lambda}_{k,(2\hat{d}_k-1)}+\hat{\lambda}_{k,2\hat{d}_k}}{2} - \hat{\sigma}^2_{k|\hat{D}_k}\right)} \quad \hat{d}_k = 1,\ldots,\hat{D}_k \tag{12}$$

Note that in (12) the estimation bias due to the noise variance is properly corrected and the two singular values associated to the same tone are averaged to reduce estimation uncertainty.

C. Coordinated Spectral Support Estimation

In this paper, the spectral support of possible sinusoidal disturbances is defined as the set of frequencies at which significant harmonics or interharmonics are detected in the majority of the K collected waveforms. It is worth emphasizing that different distributed measurement devices may return frequency and amplitude estimates at different reporting rates. Assuming that the values returned by (11)-(12) are properly time-stamped, only the estimates that can be properly aligned in time should be merged together. Under this assumption, the accuracy of the frequency estimates based on (11) depends on the ratio between the power of each sinusoidal component and the noise power level. The greater this ratio, the lower the frequency estimation uncertainty [18]. For this reason, we propose to merge the frequency estimates returned by (11) for different waveforms, but corresponding to the same component, as described below. For the sake of simplicity, in this paper, we will refer to the "prevailing" sinusoidal components as those tones that are detected in more than $K/2$ waveforms. To this purpose, the frequencies $\hat{f}_{k,\hat{d}_k}$ for all values of indexes $\hat{d}_k = 1,\ldots,\hat{D}_k$ and $k = 1,\ldots,K$ are clustered into subsets whenever the maximum difference between pairs of them is ± 1.5 Hz. Recalling that the subsets with less than $K/2$ of nearby frequency values are discarded, just $D \leq \max_k D_k$ groups of frequency values to be merged remain. Thus, the frequencies of the spectral support result from the following weighted average, i.e.

$$\hat{f}_{\hat{d}_{\rm tot}} = \frac{\sum_{k=1}^{K} \hat{f}_{k,\hat{d}_{k,\rm tot}} \frac{\hat{A}^2_{k,\hat{d}_{k,\rm tot}}}{\hat{\sigma}^2_{k|\hat{D}_k}}}{\sum_{k=1}^{K} \frac{\hat{A}^2_{k,\hat{d}_{k,\rm tot}}}{\hat{\sigma}^2_{k|\hat{D}_k}}} \quad \hat{d}_{\rm tot} = 1,\ldots,D \tag{13}$$

where $\hat{d}_{k,\rm tot}$ is the index $\hat{d}_k$ corresponding to the $\hat{d}_{\rm tot}-$th prevailing component identified in the grid. If such component is not detected in the $k-$th waveform, $\hat{A}_{k,\hat{d}_{k,\rm tot}} = 0$. It is interesting to notice that the additional computational burden of the coordinated estimation is almost negligible compared with that of the local algorithms described in Sections II-A and II-B. This is indeed dominated by the estimation and SVD computation of matrix $\mathbf{R}_k$.

III. Tests and Results

The proposed approach has been validated by performing different tests with a modified and reduced version of the 50 Hz CIGRE European Low Voltage (LV) distribution network shown in Fig. 1 [22]. The tests have been implemented in RTDS that is a power system simulator capable of reproducing the system dynamics from DC up to 3 kHz [23]. Thus, it is able to simulate realistic operating conditions even in the presence of harmonics and interharmonics. The voltage and current waveforms obtained from RTDS have been considered as the reference values. A different amount of white Gaussian noise has been added to the reference waveforms to simulate the effect of various random uncertainty contributions (e.g., due to the environment and the acquisition stage). As a consequence, in what follows, the results obtained for different values of Signal-to-Noise Ratio (SNR) are reported. The wideband noise contributions affecting the waveforms collected at different nodes are assumed to be independent.

Three measurement points on the LV side of the grid have been considered, corresponding to the red dots (buses 2, 5, and 8) in Fig. 1. Each measurement device is supposed to measure the three-phase bus voltages and the three-phase currents of an adjacent line, as indicated by the arrows in the figure.

The local detection and frequency estimation of the sinusoidal components is based on the algorithm described in Sections II-A and II-B, which is applied to every phase signal, both for voltages and currents. The coordination step is based on the merging procedure described in Section II-C and applied to the estimates collected from the three aforementioned instruments.

In this paper, the analyzed scenarios have been simulated considering the presence of harmonics in both the voltage and the current waveforms. In RTDS, the harmonics are simulated considering the joint effect of medium voltage (MV) supply and low voltage (LV) nodes distortion. Different operating conditions have been considered to assess the performance of the

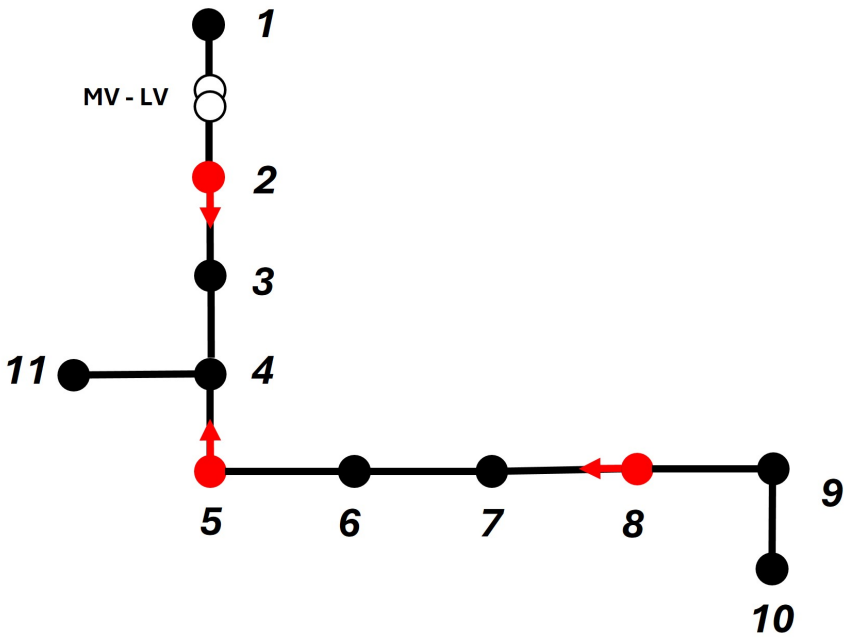

Fig. 1. Test Network, modified and reduced version of the CIGRE European LV grid.

proposed approach. The results are reported by focusing on components frequency estimation accuracy because of its relevance for spectral support estimation.

The testing set-up settings are summarized below.

- Three harmonics (of order 3, 5 and 7) have been considered in all tests.
- In a second group of tests a further interharmonic at 75 Hz has been added.
- The SNR at nodes 2 and 8 in Fig. 1 is assumed to be larger than at node 5.
- For the sake of simplicity, but with no loss of generality, the sampling rate is set to $f_{s_k} = f_s = 10$ kHz for all waveforms.
- Therefore, the number of samples per record and the data record length are also the same at all nodes, i.e., $M_k = M = 268$ and $L_k = M_k$. $N = 10^4$ measurements are collected from each device. As a result, the total duration of each experiment is about 275 s.

The first test (i.e, with harmonics only) has been carried out considering SNR $= 55$ dB at node 2 and 8 and SNR $= 65$ dB at node 5. These voltage harmonic components are injected from the MV side of the grid, namely at node 1 in Fig. 1. In addition, also an harmonic current injection at node 8 has been considered. As a result, the maximum amplitude of the 3rd, the 5th and the 7th voltage harmonic components, are about $1.5\,\%$, $0.9\,\%$ and $0.7\,\%$, respectively, of the fundamental.

As an example of the obtained estimation results, Fig. 2 shows the box-and-whiskers plots of the harmonic frequency estimation errors corresponding to the voltage waveforms. In particular, a comparison between the frequency errors achieved considering the voltage waveforms at node 8 only and those obtained from (13) is reported. In the single-node case, each frequency estimate is obtained by averaging the frequency estimates of the three phases.

The accuracy improvement achievable with the proposed approach is rather evident. For instance, focusing on the 7th harmonic, the 75th percentile of frequency error decreases from 50.8 mHz to 10.3 mHz. Moreover, while the uncertainty range using local measurement data depends only on the power of each harmonic (thus errors increase with the harmonic order in this test), in the coordinated case the range of frequency errors is rather equalized.

Similar considerations hold for current signals. Fig. 3 reports the box-and-whiskers diagrams of the frequency estimation errors associated with the 3rd, the 5th and the 7th harmonics of the current waveforms. Also in this case, the idea to aggregate the frequency estimates of different harmonics in a coordinated manner, to improve the spectral support estimation of the sinusoidal components of the current waveforms, brings about a tangible improvement. As mentioned above, the three-phase branch currents of lines $(2, 3)$, $(5, 4)$ and $(8, 7)$ are measured (the indexes indicate also the current direction).

The performance of the proposed technique has been also assessed by computing the corresponding root mean square estimation errors (RMSEs). It is important to highlight that the presented results do not include all the possible sources of uncertainty of the measurement chain (e.g., due to the measurement transducers).

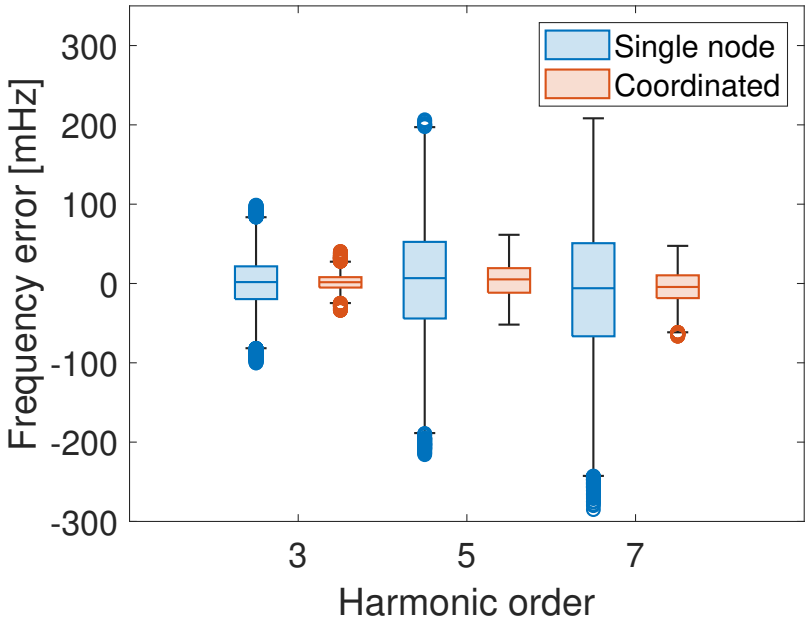

Fig. 2. Frequency estimation errors of three harmonics of the measured voltage waveforms: coordinated vs. single node (node 8) approach.

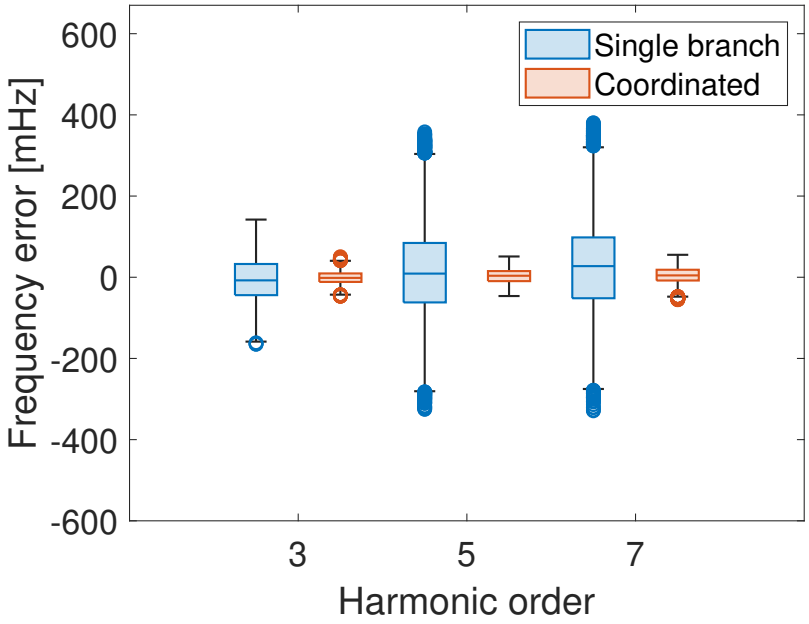

Fig. 3. Frequency estimation errors of three harmonics of the measured current waveforms: coordinated vs. single branch (branch $(8, 7)$) approach.

The quantitative comparison of the RMSE values associated with the local and coordinated estimation of voltage and current harmonic frequencies is illustrated in Table I. Observe that the RMSE values of the frequency estimates obtained with the coordinated approach are almost the same or even lower than the best RMSE values based on local measurements only. The measurement device placed at node 5 is the least affected by noise and thus it provides the most accurate frequency measurements for each harmonic order. Nevertheless, the coordinated approach leads to further improvements. In general, the RMSE values obtained with the coordinated approach are three or more times lower than those achieved with local measurements at nodes 2 and 8, although they also depend on the harmonic order, In this simple configuration, the measurement devices

TABLE I
COMPARISON OF LOCAL AND COORDINATED HARMONIC FREQUENCY ESTIMATION ERRORS WHEN BOTH VOLTAGE AND CURRENT WAVEFORMS ARE CONSIDERED

Harmonic order	Component frequency [Hz]	Method	RMSE [mHz] Voltages	RMSE [mHz] Currents
3	150	Coordinated	10.3	14.0
		Node 2	35.3	50.6
		Node 5	10.6	15.2
		Node 8	32.2	54.9
5	250	Coordinated	22.7	18.4
		Node 2	67.3	63.9
		Node 5	22.5	21.6
		Node 8	75.7	110
7	350	Coordinated	21.7	28.3
		Node 2	82.9	61.0
		Node 5	25.2	30.4
		Node 8	89.9	115

installed at nodes 2 and 8 greatly benefit from the "feedback" provided by spectral support estimation at node 5, thus confirming the potential of a coordinated monitoring scheme.

To better investigate the advantages of the proposed solution, an analogous comparison is performed by injecting an additional 75-Hz voltage interharmonic disturbance on the MV side of the grid. The interharmonic amplitude has been set equal to $40\,\%$ of the third harmonic component at the same node. Table II reports the RMSE values of the harmonic and interharmonic frequency estimates obtained using both voltage and current signals. The interhamonic component is lower than the others and its estimation is less accurate but the results confirm the advantages of introducing the coordinated approach for spectral support estimation. Indeed, the frequency estimates based on (13) are always more accurate than the local ones when current signals are considered. For voltage signals, a slight degradation with respect to the results based on local measurement can be observed at node 5 when seeking the interharmonic position in the spectrum (i.e., the most difficult to find). This is due to the fact that the coordinated spectral support estimation depends also on the estimated RMS amplitude of each component (see (13)), that is in turn affected by some uncertainty. This issue is more relevant when only few local estimates of weak components with significant differences in estimation accuracy are merged as in the proposed scenario. However, also for voltage signals, the coordinated approach tends to mitigate the frequency errors for all the other components.

In the unlikely case that the interharmonic frequency is a multiple of f_s/M_k, the performance of the local detection algorithm degrades, but it mainly affects that component only. Indeed, further tests (not reported for space constraints) revealed that all the other harmonic components are still identified correctly and their frequencies are still estimated (and merged) with good accuracy, provided that the interharmonic component amplitude is not very large, as it commonly occurs in practice.

IV. CONCLUSIONS

A critical problem in distribution systems affected by a large penetration of renewable-based generators and nonlinear loads is the high harmonic and interharmonic distortion level. Such a distortion should be estimated and, if possible, the most critical components should be compensated, e.g., by using the control features of smart power electronic converters. In this paper, we assume that various smart devices commonly deployed in distribution systems are equipped with an algorithm able to measure the frequency of the local harmonics and interharmonics affecting current and voltage waveforms. Such local estimates are then combined to estimate the spectral support of the prevailing sinusoidal disturbances over a given portion of the grid. Some tests have shown that the proposed approach is effective and feasible. This is a first step towards novel strategies for power quality improvement in active distribution grids. Future research studies will aim at improving the proposed coordinated data fusion approach through a more sophisticated clustering technique. Also, a deeper analysis of the possible uncertainty contributions is needed.

REFERENCES

[1] C.-I. Chen, Y.-C. Chen, Y.-C. Chin, and C.-H. Chen, "Integrated power-quality monitoring mechanism for microgrid," *IEEE Trans. Smart Grid*, vol. 9, no. 6, pp. 6877–6885, 2018.

[2] S. Sepasi, C. Talichet, and A. S. Pramanik, "Power quality in microgrids: A critical review of fundamentals, standards, and case studies," *IEEE Access*, vol. 11, pp. 108 493–108 531, 2023.

[3] J. Hu, Y. Shan, K. W. Cheng, and S. Islam, "Overview of power converter control in microgrids—challenges, advances, and future trends," *IEEE Trans. Power Electron.*, vol. 37, no. 8, pp. 9907–9922, 2022.

[4] F. Nejabatkhah, Y. W. Li, and H. Tian, "Power quality control of smart hybrid AC/DC microgrids: An overview," *IEEE Access*, vol. 7, pp. 52 295–52 318, 2019.

TABLE II
COMPARISON OF LOCAL AND COORDINATED HARMONIC AND INTERHARMONIC FREQUENCY ESTIMATION ERRORS

Harmonic interharmonic order	Component frequency [Hz]	Method	RMSE [mHz] Voltages	RMSE [mHz] Currents
1.5	75	Coordinated	42.5	86.7
		Node 2	116	194
		Node 5	40.7	97.0
		Node 8	146	286
3	150	Coordinated	10.1	15.9
		Node 2	40.5	56.7
		Node 5	11.6	17.4
		Node 8	34.1	59.5
5	250	Coordinated	24.8	18.7
		Node 2	70.7	70.4
		Node 5	24.6	21.4
		Node 8	77.0	112
7	350	Coordinated	20.4	25.2
		Node 2	76.6	60.9
		Node 5	22.7	25.9
		Node 8	74.2	132

[5] N. Ashraf *et al.*, "Investigation of the power quality concerns of input current in single-phase frequency step-down converter," *Appl. Sci.*, vol. 12, no. 7, pp. 1–18, 2022.

[6] X. Liang and C. Andalib Bin-Karim, "Harmonics and mitigation techniques through advanced control in grid-connected renewable energy sources: A review," *IEEE Trans. Ind. Appl.*, vol. 54, no. 4, pp. 3100–3111, 2018.

[7] P. Imgart, M. Beza, M. Bongiorno, and J. R. Svensson, "An overview of grid-connection requirements for converters and their impact on grid-forming control," in *2022 24th European Conf. on Power Electron. and Appl. (EPE'22 ECCE Europe)*, 2022, pp. 1–10.

[8] I. V. Banu *et al.*, "Passive anti-islanding protection for three-phase grid-connected photovoltaic power systems," *Int. J. of Electr. Power & Energy Syst.*, vol. 148, pp. 1–10, 2023.

[9] I. Colak, E. Kabalci, G. Fulli, and S. Lazarou, "A survey on the contributions of power electronics to smart grid systems," *Renewable and Sustainable Energy Rev.*, vol. 47, pp. 562–579, 2015.

[10] J. Benzaquen, M. Miranbeigi, P. Kandula, and D. Divan, "Collaborative autonomous grid-connected inverters: Flexible grid-forming inverter control for the future grid," *IEEE Electrific. Mag.*, vol. 10, no. 1, pp. 22–29, 2022.

[11] A. M. dos Santos Alonso, D. I. Brandao, T. Caldognetto, F. P. Marafão, and P. Mattavelli, "A selective harmonic compensation and power control approach exploiting distributed electronic converters in microgrids," *Int. J. of Electr. Power & Energy Syst.*, vol. 115, pp. 1–15, 2020.

[12] M. M. Albu, M. Sănduleac, and C. Stănescu, "Syncretic use of smart meters for power quality monitoring in emerging networks," *IEEE Trans. Smart Grid*, vol. 8, no. 1, pp. 485–492, 2017.

[13] R. Nicolosi, L. Piegari, and A. Benigni, "A smart PV inverter controller with pmu capability," in *2016 Clemson Univ. Power Syst. Conf. (PSC)*, 2016, pp. 1–7.

[14] P. Castello, C. Laurano, C. Muscas, P. A. Pegoraro, S. Toscani, and M. Zanoni, "Harmonic synchrophasors measurement algorithms with embedded compensation of voltage transformer frequency response," *IEEE Trans. Instrum. Meas.*, vol. 70, pp. 1–10, 2021.

[15] D. D. Giustina *et al.*, "Smart grid automation based on iec 61850: An experimental characterization," *IEEE Trans. Instrum. Meas.*, vol. 64, no. 8, pp. 2055–2063, 2015.

[16] W. Zhou, O. Ardakanian, H.-T. Zhang, and Y. Yuan, "Bayesian learning-based harmonic state estimation in distribution systems with smart meter and dpmu data," *IEEE Trans. Smart Grid*, vol. 11, no. 1, pp. 832–845, 2020.

[17] D. Carta, C. Muscas, P. A. Pegoraro, A. V. Solinas, and S. Sulis, "Compressive sensing-based harmonic sources identification in smart grids," *IEEE Trans. Instrum. Meas.*, vol. 70, pp. 1–10, 2021.

[18] X. Shan, D. Macii, D. Petri, and H. Wen, "Enhanced IpD2FT-based synchrophasor estimation for m class pmus through adaptive narrowband interferers detection and compensation," *IEEE Trans. Instrum. Meas.*, vol. 73, pp. 1–14, 2024.

[19] R. Roy and T. Kailath, "ESPRIT-estimation of signal parameters via rotational invariance techniques," *IEEE Trans. Acoust., Speech, Signal Process.*, vol. 37, no. 7, pp. 984–995, 1989.

[20] S. Kritchman and B. Nadler, "Determining the number of components in a factor model from limited noisy data," *Chemom. and Intell. Lab. Systems.*, vol. 94, no. 1, pp. 19–32, 2008.

[21] ——, "Non-parametric detection of the number of signals: Hypothesis testing and random matrix theory," *IEEE Trans. Signal Process.*, vol. 57, no. 10, pp. 3930–3941, 2009.

[22] K. Strunz, E. Abbasi, R. Fletcher, N. Hatziargyriou, R. Iravani, and G. Joos, *TF C6.04.02 : TB 575 – Benchmark Systems for Network Integration of Renewable and Distributed Energy Resources*. CIGRE, 2014.

[23] RTDS Technologies Inc., "Real Time Digital Simulator (RTDS)," https://www.rtds.com.